Proceedings of the 3rd International Conference on Computing Innovation and Applied Physics
DOI: 10.54254/2753-8818/34/20241125

River water injecting into sea: Movement of sediments in stable stratified flows

Suni Yao
Shanghai Pinghe School, Mingyue Rd 1029, Pudong, Shanghai, China

stephanieyao.stu@gmail.com

Abstract. The study of sediment movement in a stably stratified (each layer is less dense than the one below it) fluid is important for applications such as airborne virus transport, contaminant transport, and sediment settling in river inlets. This project will quantify the effect of sediment-driven instability on the horizontal motion of sediment in a stably stratified fluid. Experiments are designed to analyze this process by adding sediment-rich brine-free water to sediment-free brine, where salinity differences are used to construct stably stratified fluids. The experiments are done with salinity same as salty water with concentration of sediments derived from linear stability analysis. This work provide baseline experiments for sediment settling in a stably stratified fluids for numerical validations in the future.

Keywords: settling-driven instability, double-diffusive convection, stably stratified fluids

1. Introduction

PM2.5 pollutant dispersion has an important impact on people's daily life production. For example, the haze produced in Beijing in 2018 lasted for 10 days and seriously affected daily life. PM2.5 propagation in the air can also be described as sedimentation due to its small particles. Its propagation in the air is also often affected by a stably stratified density gradient, especially at night when the ground air temperature is lower and the bottom air density is higher. This stable stratification significantly affects the settling of PM2.5 in the vertical direction and its prediction of transport in the horizontal direction. Studying the movement of sediment in the stably stratified fluid can also provide accurate predictions of PM2.5 transport in the air, especially in the horizontal direction, which can be inferred to determine the source of PM2.5 and control PM2.5 reduction more precisely.

The movement of sediments in stably stratified fluids is also important for studying sediment settling in river inlets. Riverbed sediments are formed by gravitational sedimentation. The basic principle is the process by which solid particles are suspended in a fluid sink and are separated from the fluid. Relying on the action of the earth's gravitational field and the difference in density between the particles and the fluid, the relative movement occurs and settles, i.e. gravitational sedimentation. When the particles are larger, the flow velocity is more obvious, and when the particles are smaller, the flow velocity is less obvious. Since the salinity of rivers is generally much less than the salinity of seawater thus causing stable lamination, the sediment in rivers may also be affected by this buoyancy at the mouth of the sea, reducing its sedimentation rate.

Studying the stability and horizontal transport properties of sediment in stably stratified fluids is important for investigating the horizontal transport properties of aerosols and investigating the sediment

DOI: 10.54254/2753-8818/34/20241125

sinking properties in river bed inlets, and further providing a new understanding of air pollutant transport distance, and the formation mechanism of river bed inlets. In order to study the horizontal transport properties of pollutant aerosols in the atmosphere and to study the movement of sediments in the riverbed inlets, we abstracted and studied the stability and horizontal transport of sediments in the stably stratified fluids.

The mechanisms involved in sediment transport in stably stratified fluids include Rayleigh-Taylor instability [1] and double-diffusive instability [2]. Both of them may occur when a layer of freshwater containing sediment is placed above purely salty water (the model used when river water flows into the sea) [3, 4]. The Rayleigh-Taylor instability is caused when the upper fluid sediment density is higher than the lower water density. For example, this instability is common in aerosols containing viruses and in air containing PM2.5.

Stable density stratification occurs when each layer is less dense than the one below it. In nature, stably stratified boundary layers can be generated by the advection of warm air over a colder surface, as in the flow of warm air from land over colder coastal waters [5]. Radiative cooling of the ground surface, which occurs with nocturnal conditions under relatively clear skies, is the most common source of stably stratified layers. Moreover, the difference in salinity between river water and seawater causes a stable stratification of the fluid. Stable stratification can also occur in air caused by temperature differences (temperature lower at the bottom and higher at the top).

Even in the case where the overall density of the fluid is lighter on top and heavier on the bottom, double diffusion instability can arise in this problem due to the different diffusion coefficients between sediment and salt and their opposite effect on stability [6]. For example, fluids with high concentration and freshwater move down towards salty water without sediment, the freshwater will mix with the salty water, while the diffusion of sediment is a much slower process. As a result, the fluids with sediment will move downwards further leading to fingering-like structures. This is called salt-finger instability which is one important process resulting from the double-diffusive process [2].

However, there is also a significant difference between the motion of sediment in a stably stratified fluid and conventional double-diffusive convection (thermal salt convection). One of the most essential differences is that the sediment itself has a certain settling velocity. The linear stability analysis of this problem can be obtained by a spectral method with adaptive selection of grid points, and the existing literature has selected the base state profile as several step profiles [4]. Recent studies have found that this settling velocity can allow the presence of different phases in the solute at different heights, driving completely new instabilities [4, 7]. However, this instability is significantly different from the common double-diffusion convective instability, which can generate leaking mode as well as inclined waves and can significantly affect solute propagation in the horizontal direction. In seawater, the traditional double-diffusion instability leads to a fingering mode of convection when the Schmidt number (the ratio of the viscosity coefficient to the diffusion coefficient), stability ratio, and Stokes settling velocity are small. And if the Schmidt exponent, stability ratio, and Stokes settling velocity are large, the conventional double diffusion instability leads to a leaking mode of convection [8].

Two- and three-dimensional direct numerical simulations (DNS) have also explored the nonlinear motion of sediments in stable stratified fluids [9]. The initial instability growth of DNS is considered to be consistent with the most unstable flow structures predicted by linear stability analysis. The continuous elongation of individual fingers leads to secondary instabilities and finally to the formation of distinct plumes that separate from the interfacial region. Through direct numerical simulations, particles with Stokes settling velocities alter the traditional double-diffusion settling-driven fingering mode by creating an unstable nose region in a horizontal profile that lies between an upward-moving salinity and a downward-moving sediment interface. Simulation results further suggest that the double diffusion and Rayleigh-Taylor instability mechanisms result in the effective sediment settling velocity scaling with the overall buoyancy velocity of the system, which may be several orders of magnitude greater than the Stokes settling velocity [4]. The difference between the fingering-dominated and leaking modes can be seen when analyzing the power spectrum phase shift. For the case of leaking mode dominance, a phase-

DOI: 10.54254/2753-8818/34/20241125

locking mechanism is observed, which intensifies with time. Thus, the leaking mode can be interpreted as a fingering mode due to a massive flip in the nose region caused by the Rayleigh-Taylor instability [4,9].

Scaling analysis based on the results of parametric studies showed that H/l_s (height of the nose region as H and effective thickness of the salinity-sediment interface as l_s) is the key parameter that distinguishes between Rayleigh-Taylor and double-diffusion instability flow domains [4], which can be interpreted as the ratio of sediment inflow and outflow to the nose region. Direct numerical simulations show that the ratio H/l_s initially increases and then reaches a higher value depending on the balance between the double diffusion/Rayleigh-Taylor flux of sediment flowing into the noise region from above and out of the noise region below and the sediment accumulation rate within the noise region. For small values of H/l_s less than or equal to $O(0.1)$, the double diffusion instability dominates, while for larger H/l_s greater than or equal to $O(0.1)$, the sediment and salinity interfaces become increasingly separated in space and the dominant instability mode becomes a Rayleigh-Taylor mode.

This paper analyzes the stability and sediments transport in a stably stratified fluid which is settling-driven double diffusive convection. We consider both settling-driven instability and double-diffusive-driven instability. We performed a comprehensive study based on experiments, direct numerical simulations, and linear stability analysis. The density difference causing stable stratification is created by salinity. When designing the experiment, the concentration of the salt water is determined according to the results of linear stability analysis where the movement of sediments is unstable. The innovation part of the paper is that different approaches to simulating the phenomena when river fresh water is injected into salty seawater including linear stability analysis, DNS, and experiments. Results of experiments and DNS are complemented and they are used to compare the results represented in linear stability analysis.

2. Problem Setup

We first set up a model within a doubly periodic domain (modeling unbounded domain) of fluid that is initially at rest. There are 2 scalar factors, the salinity scalar $S(x,z,t)$ which diffuses at a different rate from the concentration of sediments $C(x,z,t)$, both linearly affecting the density. The overall density is stably stratified while the sediment concentration field is unstably stratified.

2.1. Governing Equations

First, we use the two-dimensional Navier-Stokes equation under *Boussinesq* approximation, which assumes density variation is small everywhere except in the buoyancy term that drives the fluid motion. $\left(\frac{\partial \boldsymbol{u}}{\partial t}+\boldsymbol{u}\cdot\boldsymbol{\nabla}\boldsymbol{u}\right)=\nu\nabla^2\boldsymbol{u}-\boldsymbol{\nabla}p-\frac{\rho-\rho_m}{\rho_m}g\boldsymbol{e}_z,\ \ \boldsymbol{\nabla}\cdot\boldsymbol{u}=0$, where $\boldsymbol{u}=(u,w)$ represents the fluid velocity vector, ν represents the kinematic viscosity of the fluid, p denotes the pressure and ρ_m is a reference density value, $\boldsymbol{e}_z$ indicates the unit vector in the z-direction. The density of the fluid ρ is dependent linearly on the salinity and concentration of the sediment as $\rho=\rho_m(1-\alpha(\underline{S}-S_m)+\beta(\underline{C}-C_m))$, where S_m and C_m are the reference values of salinity and concentration and the coefficients α and β reflect the dependence of the density on the salinity and sediment concentration, respectively. Thus, we have momentum equation as

$$\left(\frac{\partial \boldsymbol{u}}{\partial t}+\boldsymbol{u}\cdot\boldsymbol{\nabla}\boldsymbol{u}\right)=\nu\nabla^2\boldsymbol{u}-\boldsymbol{\nabla}p+[\alpha(\underline{S}-S_m)-\beta(\underline{C}-C_m)]g\boldsymbol{e}_z, \tag{1}$$

The salinity and sediment concentration fields are controlled by the advection-diffusion transport equations

$$\frac{\partial \underline{S}}{\partial t}+\boldsymbol{u}\cdot\boldsymbol{\nabla}\underline{S}=\kappa_S\nabla^2\underline{S}, \tag{2}$$

$$\frac{\partial \underline{C}}{\partial t}+\boldsymbol{u}\cdot\boldsymbol{\nabla}\underline{C}-W_{st}^*\frac{\partial \underline{C}}{\partial z}=\kappa_C\nabla^2\underline{C}, \tag{3}$$

in which constant κ_S and κ_C represents the salinity and sediment diffusivities, respectively. W_{st}^* is the constant Stokes settling velocity for the sediment.

DOI: 10.54254/2753-8818/34/20241125

In the base state, we investigate the linear stability of the fluid at rest. The salinity and sediment concentration fields in the base state depend linearly on the horizontal x and vertical z directions

$$\underline{S}(x,z,t) = S_{0z}z + S(x,z,t), \tag{4}$$
$$\underline{C}(x,z,t) = (C_{0z}z + W_{st}^{*}t) + C(x,z,t), \tag{5}$$

in which S_{0z}, C_{0z} are constants. C_0 is linear to time instead of being a constant because of the settling. However, the base state concentration gradient is constant in time.

2.2. Characteristic Scales

To non-dimensionalize the equations in §2.1, we use the standard characteristic scales of double-diffusive flow as reviewed by [2]. As a length scale, we choose our expected finger width as $[d] = (\frac{\kappa_S \upsilon}{g\alpha S_{0z}})^{\frac{1}{4}}$, where S_{0z} is the magnitude of the vertical salinity gradient in the base state. We obtain $[t] = \frac{d^2}{\kappa_S}, [u] = \frac{\kappa_S}{d}, [S] = S_{0z}d, [C] = \frac{\alpha}{\beta}S_{0z}d$ as characteristic scales for time t, velocity u, salinity S and sediment concentration C, respectively.

Thus, we can derive the following system of governing dimensionless equations for the heat-sediment system

$$\frac{1}{Pr}\left(\frac{\partial \boldsymbol{u}}{\partial t} + \boldsymbol{u}\cdot\boldsymbol{\nabla}\boldsymbol{u}\right) = \nabla^2\boldsymbol{u} - \nabla p + (S-C)\boldsymbol{e}_z, \tag{6}$$
$$\frac{\partial S}{\partial t} + \boldsymbol{u}\cdot\boldsymbol{\nabla}S + w = \nabla^2 S, \tag{7}$$
$$\frac{\partial C}{\partial t} + \boldsymbol{u}\cdot\boldsymbol{\nabla}C - W_{st}\frac{\partial C}{\partial z} + \frac{w}{R_\rho} = \tau\nabla^2 C, \quad \boldsymbol{\nabla}\cdot\boldsymbol{u} = 0 \tag{8}$$

where all quantities have now been non-dimensionalized. The dimensionless parameters in the form of the Prandtl number Pr, the diffusivity ratio τ and the settling velocity W_{st} are defined as $Pr = \frac{\upsilon}{\kappa_S}, \tau = \frac{\kappa_C}{\kappa_S}, W_{st} = \frac{W_{st}^{*}d}{\kappa_S}$. We also use the density ratio $R_\rho = \frac{\alpha S_{0z}}{\beta C_{0z}}$ to measure the relative strength of the stabilizing vertical salinity gradient and the destabilizing vertical sediment gradient in the base state [10].

2.3. Data Measurement

To measure different particles' settling velocities, we do not expect to use a large water tank. Instead, it is enough to use smaller equipment. Here we use glass jars which are more convenient.

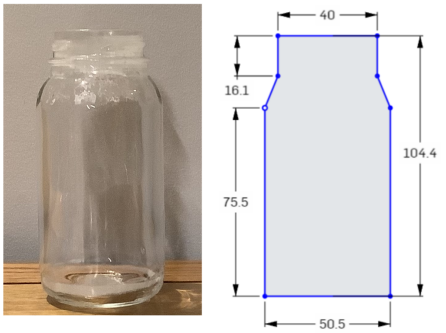

(a) The bottle used for measuring settling velocity
(b) The scale of the bottle

Figure 1. Glass jar used to measure the settling velocity and the scale of the jar.

DOI: 10.54254/2753-8818/34/20241125

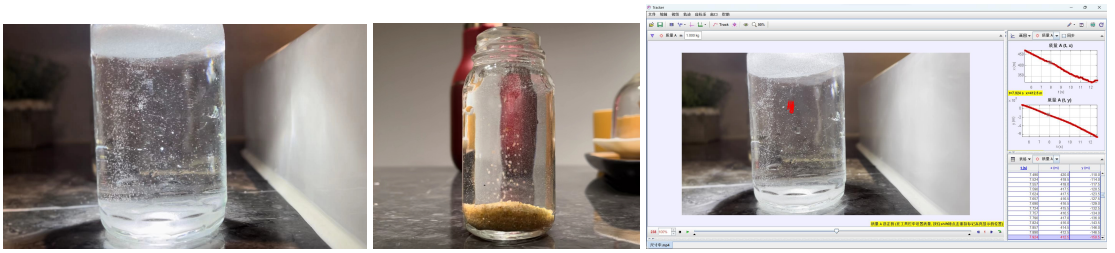

(a) 50-100 μm PMMA (b) 500-1000 μm gravel (c)

Figure 2. a: Screenshots of videos that record particles' settling process. b: Screenshot of plotting position to time $x, y - t$ graph using Tracker. The position of sediments is labeled every time within 1 frame. Then the measured values were pasted to Logger Pro to replot the $y - t$ graph and find the linear fit of the graph.

Then, to calculate the settling velocity, we first fill most parts of the jar with water, then pour sediments into the jar at a low height so that the initial velocity does not affect the settling velocity's measurement much. At the same time, record a video clip of the experiment. After sediments end up settling down, we use the video and track a specific particle in sediments. Then we can plot a diagram with the independent variable t and dependent variable displacement y. Therefore, the gradient of this function should be the settling velocity. Also, to be noted, in order to reduce the errors, track at least 3 different particles of the same sediment.

Besides, to measure the volume of the particles, I first plan to add particles in the glass jar and then put water in the glass jar until the jar is full. Measure the mass of water and therefore get the volume of water. The volume of particles can be calculated by the capacity of the jar subtracted from the volume of water. However, when we pour water into the jar, it is discovered that the particles and water are easy to overflow. Instead, changing the turns, which is to put particles in water is better to control. Also, calculate the mass by looking at the change of mass during the process of adding particles. Therefore, we can successfully derive the density of particles.

2.4. Quantities Measurement and Calculation

First, we put gravel and PMMA particles into glass jars and then take videos of the settling process. Then the software Tracker is used to track the settling motion of 3 fixed particles of every sediment. Here we take PMMA particles as an example, we can get the settling velocity with dimensions $W_{st}^* = 0.015083$ m/s downwards. 1

By the same method, we can also derive the settling velocity with dimensions for Sediments 2 and 3.

For this work, we use salinity to perform the stable stratification, and thus $\kappa_T = 0.145 \times 10^{-8}$ m^2/s, $\alpha = 0.76 \times 10^{-3}$ PSU^{-1}. Here, S only represents some component that is stably stratified, which is salt in current work and to simulate the environment in salt water, S_{0z} is set to be 35 PSU/0.05 m.

According to §2.2, to get other quantities, we need to first calculate the expected finger width which is

$$[d] = \left(\frac{\kappa_T \upsilon}{g\alpha T_{0z}}\right)^{1/4} = \left(\frac{0.145 \times 10^{-8}\ \text{m}^2/\text{s} \times 10^{-6}\ \text{m}^2/\text{s}}{9.8\ \text{m/s}^2 \times 0.76 \times 10^{-3}\ (\text{PSU})^{-1} \times 35\ \text{PSU}/0.05\ \text{m}}\right)^{1/4} = 1.2914 \times 10^{-4}\ \text{m} \tag{9}$$

$$[u] = \frac{\kappa_S}{[d]} = \frac{0.145 \times 10^{-8}\ \text{m}^2/\text{s}}{1.2914 \times 10^{-4}\text{m}} = 1.1228 \times 10^{-5}\ \text{m/s} \tag{10}$$

DOI: 10.54254/2753-8818/34/20241125

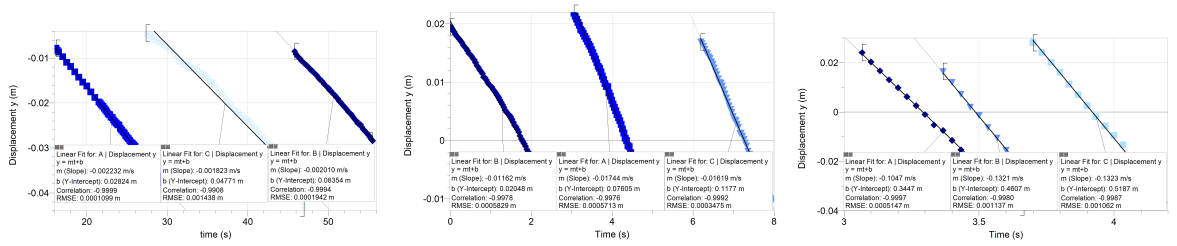

Figure 3. Left: Particle 1 (50-100 μm PMMA): The settling velocity with dimensions is the gradient of the displacement $y - t$. By tracking 3 separate sediment particles A, B, C with settling velocity 0.002232 m/s, 0.001823 m/s and 0.002010 m/s relatively, the settling velocity $W_{st}^* = 0.002021$ can be got by calculating the average of the separated settling velocities with dimensions. Middle: Particle 2 (200-500 μm PMMA): Similarly, we track sediment particles A, B, C with settling velocity of 0.01744 m/s, 0.01162 m/s and 0.01619 m/s relatively. The average settling velocity W_{st}^* should be 0.015083 m/s. Right: Particle 3 (500-1000 μm gravel): Similarly, with 0.1047 m/s, 0.1321 m/s and 0.1323 m/s as relative settling velocity for A, B, C, the average settling velocity is 0.123325 m/s.

Also, compute τ following the paper by [11].

$$\tau = \frac{k_B T_m}{6\pi\rho_m v r \kappa_S} + \zeta \frac{r W_{st}^*}{\kappa_S} = \frac{k_B T_m}{6\pi\rho_m v r \kappa_S} + \zeta \frac{r}{d} W_{st} \tag{11}$$

where $k_B = 1.380649 \times 10^{-23} \mathrm{m}^2\ \mathrm{kg}\ \mathrm{s}^{-2}\ \mathrm{K}^{-1}$ is the Boltzmann Constant, T_m is room temperature, r is the radius of the particles, ζ is a factor of order unity that depends on the volume fraction, e.g. [12].

Here we list Table 1 of sediments and their corresponding W_{st} and τ. Here we use the geometric mean of τ to do further calculations because a significant difference exists between the results in Table 2: $\tau_1 = \sqrt{69.7 \cdot 139.4} = 98.6$, $\tau_2 = \sqrt{2080.5 \cdot 5201.2} = 3289.5$, $\tau_3 = \sqrt{42422 \cdot 84845} = 59994$.

Table 1. In the table, we show W_{st} and τ of sediments with different radii.

Particles and Radius	W_{st}	τ
Sediment 1 (PMMA 50-100 μm)	180.05	$69.7 - 139.4$
Sediment 2 (PMMA 200-500 μm)	1343.37	$2080.5 - 5201.2$
Sediment 3 (gravel 500-1000 μm)	10957	$42422 - 84845$

Table 2. Sediments with different radii. W_{st}, $\bar{W}_{st}$, τ, ρ, β are listed.

Particles and Radius	W_{st}	$\bar{W}_{st}$	τ	ρ	β
Sediment 1 (PMMA 50-100 μm)	180.05	11.25-45	98.6	1.01	0.50249
Sediment 2 (PMMA 200-500 μm)	1343.37	180-1125	3289.5	1.03	0.50739
Sediment 3 (gravel 500-1000 μm)	10957	1125-4500	59994	2.47	0.71182

The geometric mean of τ will be used to analyze linear stability. We also introduce another way of calculating a theoretical value of W_{st}, marked as $\bar{W}_{st}$ using experiment formula according to [11]:

$$\bar{W}_{st} \simeq 0.45 \left(\frac{r}{10\mu m} \right)^2 \tag{12}$$

DOI: 10.54254/2753-8818/34/20241125

This theoretical value of W_{st} can be used to comment on the value of W_{st} we got from the experiment. We list another table for some useful parameters (W_{st}, $\bar{W}_{st}$, τ, R_ρ, β).

In this table, we can also compare the magnitude of W_{st} and the theoretical value $\bar{W}_{st}$. All values of W_{st} are larger than the corresponding theoretical one. Hopefully, the error between the theoretical and experiment values isn't very significant.

Measure the density of particles, and obtain β for the particle, $\beta = \frac{1}{\rho_w} \times \frac{1}{\frac{1}{\rho_w}+\frac{1}{\rho_p}} = \frac{1}{1+\rho_w/\rho_p}$. Here, concentration is measured as $C = \frac{\text{g of particle}}{\text{g of water}}$. We designed several groups of different concentration differences. Then, we compute several different density ratios for each particle. For stable stratification by salt, just keep 35 PSU to model the seawater. Here we provide a list of several density ratios, covering both $R_\rho < 1/\tau$ and $R_\rho > 1/\tau$, even though the relation between R_ρ and $1/\tau$ is only suitable for the condition without settling velocity and is not obvious when settling velocity $W_{st} \neq 0$ as shown in [13]. We should set $Pr = 700$ corresponding to salt in water in all of the numerical simulations.

3. Methodology

3.1. Experiment Setup

The major piece of equipment that evolved during the investigation is shown in Figure 4. My apparatus design is based on the apparatus used by [14].

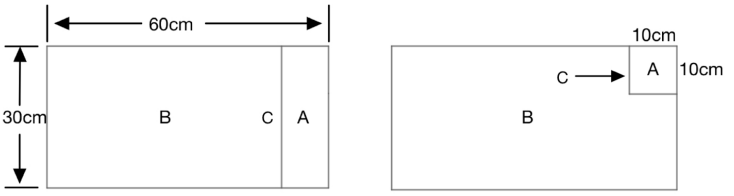

Figure 4. Structure and dimensions of the acrylic tank with reservoir (top and front views from left to right): Zone A is used for freshwater containing sediment, and Zone B is a clear saltwater solution. A and B are separated by a well-sealed and removable acrylic bulkhead C. The total tank size is 60cm*30cm*30cm, the A area is 10cm wide and 10cm deep, the rest is the B area, and the acrylic bulkhead size is 10cm$\times$ 30cm.

At the start of the experiment, the main tank B was filled with a sodium chloride solution, and the density ρ was measured to five decimal places. The secondary box A was filled with a well-mixed and known volume of particle-laden interstitial fluid (e.g., we use fresh water here) that had been prepared by adding a known weight of particles (m_P) to a known weight of fluid (m_I). The weight concentration of sediment was $c = \frac{m_P}{m_P+m_I}$, so that the density of the mixture (ρ_C) could be derived using $\frac{1}{\rho_C} = \frac{c}{\rho_P} + \frac{1-c}{\rho_I}$, where ρ_I is the density of fresh water, ρ_P is the density of the particles. We use polymethyl methacrylate (PMMA) polymers of 200-500 μm which is the most fit size to simulate the sediments in the river.

To investigate the fluid dynamical movement in the experiment, barrier C was removed after a final thorough stirring of the smaller water tank A for 1-2 seconds to ensure that the sediments did not settle to the bottom of tank A. The motion of the current was recorded on videotape and then analyzed using Tracker to compute the settling velocity of the sediments.

The size of sediments in rivers is about 0.0742 mm, and we planned to use acrylic powder particles ranging from 0.2-0.5 mm for the experiment. The concentration of salt in seawater is about 3.5%, so we will add sodium chloride which is 3.5% of the total mass to simulate the ocean's environment.

DOI: 10.54254/2753-8818/34/20241125

4. Results

4.1. Experiment Observation

Since density ratio R_ρ is defined by $R_\rho = \dfrac{\alpha S_{0z}}{\beta C_{0z}}$, where C_{0z} and S_{0z} are the magnitudes of vertical sediment concentration gradient and salinity gradient in the base state, respectively, and for simulating the environment in seawater, we set C_{0z} as the fixed value 35 PSU/0.3m and S_{0z} can be expressed as $S_{0z} = \dfrac{R_\rho \beta \cdot C_{0z}}{\alpha}$ while $\alpha = 0.76 \times 10^{-3}$ PSU^{-1}, we determine the magnitude of S_{0z} to remain their R_ρ corresponding to our linear stability analysis results in Table 3.

Table 3. This table lists the value of parameters that can be achieved in experiments. Some situations with small magnitudes of R_ρ cannot be achieved because C_{0z} will be unexpectedly large and rarely appear in reality.

Sediment	C_{0z}	S_{0z}	β	R_ρ	$R_\rho\beta/\alpha$
Sediment 1	5.30 PSU/0.3 m	35 PSU/0.3 m	0.50249	0.01	6.61
Sediment 2	5.24 PSU/0.3 m	35 PSU/0.3 m	0.50739	0.01	6.68
Sediment 3	3.74 PSU/0.3 m	35 PSU/0.3 m	0.71182	0.01	9.37

Instead of matching all numerical values of R_ρ that are listed in Table 4 and simulated, here we only present the experiments with $R_\rho = 0.01$ because in this condition, the experiment phenomenon is the most obvious.

Table 4. Here we choose different values for the density ratio for different sediments. Also, for the case when $R_\rho > 1/\tau$, we all choose 1 to compare the results when R_ρ is fixed.

Particles and Radius	W_{st}	τ	R_ρ
Sediment 1 (PMMA 50-100 μm)	180.05	98.6	0.01, 1, 1.5
Sediment 2 (PMMA 200-500 μm)	1343.37	3289.5	0.00001, 0.01, 1
Sediment 3 (Gravel 500-1000 μm)	10957	59994	0.000001, 0.01, 1

The photos of the experiments that are shown in Figure 5, 6, 7 are recorded by the camera. The experiment consists of three parts: the water tank, lighting support, and the data recording camera. A general view of the experiment is shown in Figure 8 (left), and a front view photo of the water tank is provided in Figure 8 (right).

DOI: 10.54254/2753-8818/34/20241125

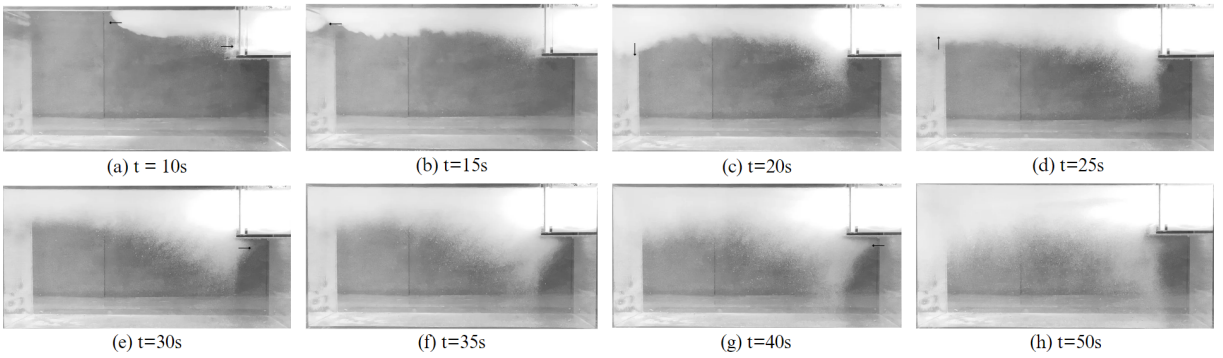

Figure 5. Photographs of a sedimenting current for Sediment 1 (PMMA 50-100 μm) with $R_\rho = 0.01$. From (a) to (h) it shows the significant movement of sediments in the time period from t = 10s to t = 50s. Arrows in graphs show the general movement of the sediments.

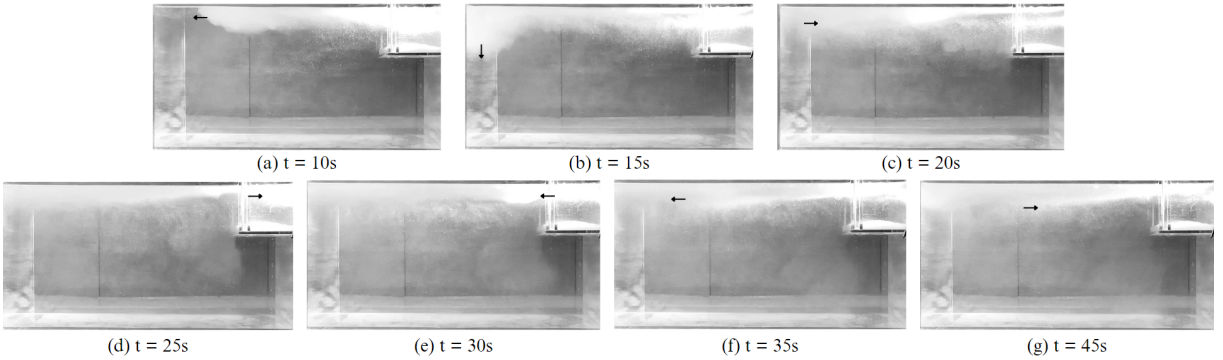

Figure 6. Photographs of a sedimenting current for Sediment 2 (PMMA 200-500 μm) with $R_\rho = 0.01$. From (a) to (g) it shows the significant movement of sediments in the time period from t = 10s to t = 50s.Arrows in graphs show the general movement of the sediments.

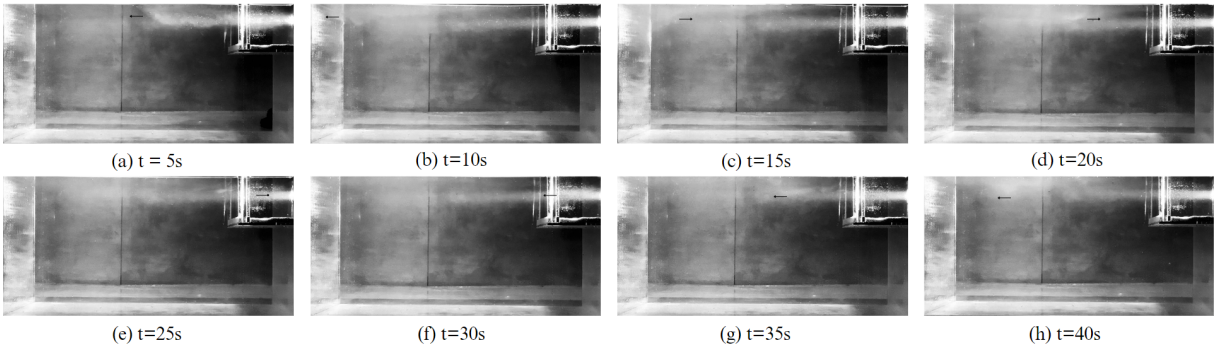

Figure 7. Photographs of a sedimenting current for Sediment 3 (Gravel 500-1000 μm) with $R_\rho = 0.01$. From (a) to (g) it shows the significant movement of sediments in the time period from t = 10s to t = 50s.Arrows in graphs show the general movement of the sediments.

DOI: 10.54254/2753-8818/34/20241125

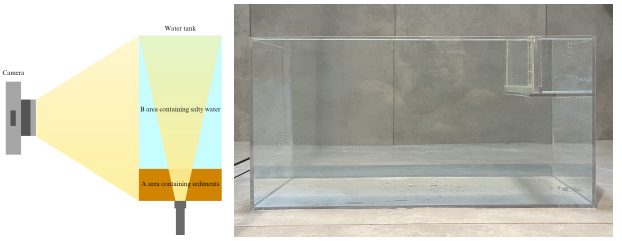

Figure 8. Left: The top view of the whole experiment system. Right: The water tank with Zone A and Zone B filled with fresh water and salty water, respectively. The sediments are not put into Zone A yet.

For Sediment 1 with $R_\rho = 0.01$, the process of spreading of sediments is shown in Figure 5, and position with visibly general movement is marked with arrows. When the removable bulkhead C was taken out, the sediment from the bottom of Zone A shifted upwards and moved horizontally. Instead, the bottom of Zone A was filled with salty water, as significantly shown in Figure 5(a) when $t = 10$ s. From 10s to 15s, the flow mainly moves leftwards without settling down. The left part of the horizontal flow reached the acrylic plate and the left part sediments moved downwards. However, it moved upwards. Another interesting phenomenon is that some sediments that are not involved in the horizontal flow, with a small initial velocity, first moved to the contact part with Zone A and then settled down when t =30-40 s, while after the 40 s the concentration of sediments with similar movement declined, as shown in Figure 5(h), with a backflow.

For Sediment 2 (PMMA 200-500 μm) with $R_\rho = 0.01$, the movement of sediments are shown in Figure 6 (middle), and for some significant movements of sediments other than basic settling are marked with arrows. Similarly to Sediment 1, after the bulkhead is removed, in Zone A the upper layer moved horizontally to the left, and the lower layer was filled by denser salty water. Also, when the sediments reached the wall, they first moved downwards and then returned moving rightwards.

With the help of a flashlight, where the concentration of sediments is larger will be brighter and easier to observe the horizontal flow. While observing Sediment 2, the horizontal movement is more dominant to Sediment 1. In total, at least 4 total back-and-forth horizontal movements can be observed clearly in 130s. Among them, 23s, 28s, 32s, and 44s are the time required for each round-trip, implying that the speed of horizontal flow declines, and after 130s, no evident horizontal flow can be observed. Other than horizontal movement, the dominant mode is elevator mode, as fingers can be observed vertically.

For Sediment 3 (Gravel 500-1000 μm) with $R_\rho = 0.01$, the movement of sediments shown in Figure 7 (right) is not obvious, mainly because the density of gravel and settling velocity are larger than PMMA particles. Most particles settle down on the bottom of Zone A and cannot move out after the bulkhead is removed. However, a small amount of less dense gravel can still come out of Zone A and move mainly horizontally, with no significant movement in the vertical direction. In addition, only 1.5 back-and-forth movements in the vertical direction in the first 40s can be observed before decaying into scattered and less rapid horizontal and vertical movements. This corresponds to the increasing wavelengths and decreasing wave number. The phenomenon is not obvious in this set of experiments, mainly because the initial flow velocity of the water is not enough and thus causes the kinetic energy not to carry most of the sediments in the horizontal movement.

5. Conclusion

In this research, we investigate the dynamics of freshwater-saltwater interactions when freshwater, carrying various sediment sizes is injected into a saline environment with a salinity of 35 PSU, which is the concentration of salt in seawater. Also, to simulate the sediments in seawater, we use particles with 50-100 μm, 200-500 μm, and 500-1000 μm sizes and also different densities controlled by the type of sediments involving PMMA particles and gravel. Our aim is to understand the stability of the resulting

DOI: 10.54254/2753-8818/34/20241125

stratified system and explore the influence of key parameters, for example, radius, density, and settling velocity with dimensions in the research.

Moving forward, future research can expand upon the synergy between experimental and numerical investigations, especially in cases where hardware constraints limit the scope of numerical simulations, such as those involving larger W_{st} and τ. Furthermore, conditions where $R_\rho = 0.01$, resulting in infinite kinetic energy modes in DNS, could be explored more extensively through experiments to provide comprehensive comparisons and verification. Additionally, addressing the challenges associated with low sediment concentrations at high R_ρ values in experiments may yield valuable insights. This comprehensive approach, where experiments and DNS complement each other, further validates the conclusions drawn from the linear stability analysis and enhances the overall robustness of the study's findings.

References

[1] Sharp D H 1984 *Physica D: Nonlinear Phenomena* **12** 3–18
[2] Radko T 2013 *Double-diffusive convection* (Cambridge University Press)
[3] Maxworthy T 1999 *Journal of Fluid Mechanics* **392** 27–44
[4] Burns P and Meiburg E 2012 *Journal of fluid mechanics* **691** 279–314
[5] Smedman A S, Tjernström M and Högström U 1993 *Boundary-layer meteorology* **66** 105–126
[6] Ouillon R, Edel P, Garaud P and Meiburg E 2020 *Journal of Fluid Mechanics* **901**
[7] Oliveira R M and Meiburg E 2018 *Journal of Fluid Mechanics* **843**
[8] Burns P and Meiburg E 2016 Double-diffusive sedimentation *International Symposium on Stratified Flows, 1 (1)*
[9] Burns P and Meiburg E 2015 *Journal of Fluid Mechanics* **762** 156–195
[10] Turner J S 1979 *Buoyancy effects in fluids* (Cambridge university press)
[11] Reali J, Garaud P, Alsinan A and Meiburg E 2017 *Journal of Fluid Mechanics* **816** 268–305
[12] Segre P N, Liu F, Umbanhowar P and Weitz D A 2001 *Nature* **409** 594–597
[13] Alsinan A, Meiburg E and Garaud P 2017 *Journal of Fluid Mechanics* **816** 243–267
[14] Green T 1987 *Sedimentology* **34** 319–331